The Astrophysical Journal Letters, 765:L13 (6pp), 2013 March 1 doi:10.1088/2041-8205/765/1/L13

A *HERSCHEL* SURVEY OF THE [N II] 205 μm LINE IN LOCAL LUMINOUS INFRARED GALAXIES: THE [N II] 205 μm EMISSION AS A STAR FORMATION RATE INDICATOR*

Yinghe Zhao (赵应和)[1,2,3], Nanyao Lu[2], C. Kevin Xu[2], Yu Gao (高煜)[1,3], S. Lord[2], J. Howell[2], K. G. Isaak[4], V. Charmandaris[5,6,7], T. Diaz-Santos[8], P. Appleton[2], A. Evans[9,10], K. Iwasawa[11], J. Leech[12], J. Mazzarella[2], A. O. Petric[13], D. B. Sanders[14], B. Schulz[2], J. Surace[8], and P. P. van der Werf[15]

[1] Purple Mountain Observatory, Chinese Academy of Sciences, Nanjing 210008, China; yhzhao@ipac.caltech.edu
[2] Infrared Processing and Analysis Center, California Institute of Technology, MS 100-22, Pasadena, CA 91125, USA
[3] Key Laboratory of Radio Astronomy, Chinese Academy of Sciences, Nanjing 210008, China
[4] ESA Astrophysics Missions Division, ESTEC, PO Box 299, 2200 AG Noordwijk, The Netherlands
[5] Department of Physics and ITCP, University of Crete, GR-71003 Heraklion, Greece
[6] IESL/Foundation for Research and Technology—Hellas, GR-71110 Heraklion, Greece
[7] Chercheur Associé, Observatoire de Paris, F-75014 Paris, France
[8] Spitzer Science Center, California Institute of Technology, MS 220-6, Pasadena, CA 91125, USA
[9] Department of Astronomy, University of Virginia, 530 McCormick Road, Charlottesville, VA 22904, USA
[10] National Radio Astronomy Observatory, 520 Edgemont Road, Charlottesville, VA 22903, USA
[11] ICREA and Institut de Ciències del Cosmos (ICC), Universitat de Barcelona (IEEC-UB), Martí i Franquès 1, E-08028 Barcelona, Spain
[12] Department of Physics, University of Oxford, Denys Wilkinson Building, Keble Road, Oxford OX1 3RH, UK
[13] Astronomy Department, California Institute of Technology, Pasadena, CA 91125, USA
[14] Institute for Astronomy, University of Hawaii, 2680 Woodlawn Drive, Honolulu, HI 96822, USA
[15] Leiden Observatory, Leiden University, PO Box 9513, 2300 RA Leiden, The Netherlands
Received 2012 December 11; accepted 2013 January 30; published 2013 February 14

ABSTRACT

We present, for the first time, a statistical study of [N II] 205 μm line emission for a large sample of local luminous infrared galaxies using *Herschel* Spectral and Photometric Imaging Receiver Fourier Transform Spectrometer (SPIRE FTS) data. For our sample of galaxies, we investigate the correlation between the [N II] luminosity ($L_{[\mathrm{N\,II}]}$) and the total infrared luminosity (L_{IR}), as well as the dependence of $L_{[\mathrm{N\,II}]}/L_{\mathrm{IR}}$ ratio on L_{IR}, far-infrared colors (*IRAS* f_{60}/f_{100}), and the [O III] 88 μm to [N II] luminosity ratio. We find that $L_{[\mathrm{N\,II}]}$ correlates almost linearly with L_{IR} for non-active galactic nucleus galaxies (all having $L_{\mathrm{IR}} < 10^{12}\,L_{\odot}$) in our sample, which implies that $L_{[\mathrm{N\,II}]}$ can serve as a star formation rate tracer which is particularly useful for high-redshift galaxies that will be observed with forthcoming submillimeter spectroscopic facilities such as the Atacama Large Millimeter/submillimeter Array. Our analysis shows that the deviation from the mean $L_{[\mathrm{N\,II}]}$–L_{IR} relation correlates with tracers of the ionization parameter, which suggests that the scatter in this relation is mainly due to the variations in the hardness, and/or ionization parameter, of the ambient galactic UV field among the sources in our sample.

Key words: galaxies: evolution – galaxies: ISM – galaxies: starburst – infrared: ISM

Online-only material: color figures

1. INTRODUCTION

The star formation rate (SFR) is one of the fundamental physical parameters for characterizing galaxies. Having an effective way to derive SFRs for galaxies spanning a large range of look-back times is crucial for our understanding of galaxy evolution leading back to initial conditions. Currently, SFRs have been inferred using continuum or spectral line emission from a wide range of wavelengths (e.g., Calzetti et al. 2009 and references therein; Kennicutt & Evans 2012). However, few of these SFR indicators can be observed over a large redshift range using current facilities. Using the capabilities of the ESA *Herschel Space Observatory* (hereafter *Herschel*; Pilbratt et al. 2010), it is possible to define new SFR indicators in the far-infrared (FIR) window, which can be followed up by the Atacama Large Millimeter/submillimeter Array (ALMA) over a large redshift range.

The [N II] 205 μm line, which arises from the $^3P_1 \rightarrow {}^3P_0$ transition (205.197 μm; hereafter [N II] (1→0)) of the ground state of the singly ionized nitrogen, is expected to be an excellent indicator of SFR. This FIR line emission essentially traces all of the warm ionized interstellar medium (ISM). The ionization potential of nitrogen (14.53 eV) is only ∼0.9 eV larger than that of hydrogen (13.6 eV), allowing the [N II] luminosity to be used as an estimate of the flux of ionizing photons (e.g., Bennett et al. 1994). The critical density of [N II] (1→0) is only 44 cm^{-3} at $T = 8000$ K (Oberst et al. 2006), and the energy level that emits the line corresponds to only 70 K, so that it can be easily collisionally excited. In addition, the [N II] 205 μm emission is usually optically thin because of its small Einstein coefficient, and suffers much less dust extinction than optical and near-infrared lines. In particular, this line is accessible using ALMA for a significant fraction of the $0.6 \lesssim z \lesssim 16$ redshift range (bands 3–10).[16] For more local galaxies, the [N II] (1→0) line can be observed in the two windows around 200 μm (1.25–1.4 THz and 1.45–1.6 THz; e.g., Paine et al. 2000; Yang et al. 2010) from the very driest sites with future facilities such as the Submm/THz telescope at the Chinese Antarctic Observatory under development (e.g., Cui 2010).

* *Herschel* is an ESA space observatory with science instruments provided by European-led Principal Investigator consortia and with important participation from NASA.

[16] Redshift intervals corresponding to different ALMA receivers: $11.6 \lesssim z \lesssim 16.3$ (band 3); $3.0 \lesssim z \lesssim 10.6$ (bands 4–7); $2.0 \lesssim z \lesssim 2.7$ (band 8); $1.0 \lesssim z \lesssim 1.4$ (band 9); $0.6 \lesssim z \lesssim 0.8$ (band 10).

Early studies have shown that the [N II] 205 μm line is comparatively bright. In most normal star-forming galaxies, it is the third to fifth brightest FIR/submillimeter line after [C II] 158 μm, [O III] 88 μm, [O I] 63 μm, and [N II] 122 μm lines (e.g., Wright et al. 1991; Brauher et al. 2008). The luminosity of [N II] 205 μm line ($L_{[\rm N\,II]}$) may be up to $\sim 10^{-4}$ times the total infrared luminosity ($L_{\rm IR}$). For example, $L_{[\rm N\,II]}$ is about $3 \times 10^{-4} L_{\rm IR}$ and $5 \times 10^{-5} L_{\rm IR}$ in the Milky Way (Wright et al. 1991) and M82 (Petuchowski et al. 1994), respectively. With such a high luminosity, this line has already been detected with ALMA (e.g., Nagao et al. 2012; $z = 4.76$), and IRAM 30 m (e.g. Combes et al. 2012; Decarli et al. 2012; lensed objects) for luminous/ultraluminous infrared galaxies at high redshift.

The [N II] 205 μm line is generally inaccessible to ground-based facilities, and its rest wavelength is longer than the cutoff of the *Infrared Space Observatory* (*ISO*) Long Wavelength Spectrometer (LWS). Therefore, this line was observed in only a handful of extragalactic objects using satellite and airborne platforms (e.g., Wright et al. 1991; Petuchowski et al. 1994; Lord et al. 1995) prior to the advent of *Herschel*. Here we report our first results on the [N II] 205 μm line emission for a large sample of galaxies, observed with the Fourier Transform Spectrometer (FTS) of the Spectral and Photometric Imaging Receiver (SPIRE) instrument (Griffin et al. 2010) on board *Herschel*. We present the correlation between $L_{[\rm N\,II]}$ and $L_{\rm IR}$, to characterize the [N II] 205 μm line as an SFR indicator. We also investigate possible dependences of [N II] 205 μm to IR luminosity ratio ($L_{[\rm N\,II]}/L_{\rm IR}$) on $L_{\rm IR}$, FIR color (f_{60}/f_{100}, where f_{60} and f_{100} are the *IRAS* 60 μm and 100 μm fluxes, respectively), and the [O III] 88 μm to [N II] 205 μm emission ratio ($L_{[\rm O\,III]}/L_{[\rm N\,II]}$), to reveal the cause of the scatter in this relation. Throughout the Letter, we adopt a Hubble constant of $H_0 = 70\,{\rm km\,s^{-1}\,Mpc^{-1}}$, $\Omega_{\rm M} = 0.3$, and $\Omega_\Lambda = 0.7$.

2. SAMPLE, OBSERVATIONS, AND DATA REDUCTION

The sample discussed in this Letter is part of the *Herschel* open time project *Herschel Spectroscopic Survey of Warm Molecular Gas in Local Luminous Infrared Galaxies (LIRGs)* (PI: N. Lu), which aims primarily at studying the dense and warm molecular gas properties of 125 LIRGs ($L_{\rm IR} \equiv L(8\text{–}1000\,\mu{\rm m}) > 10^{11} L_\odot$, where $L_{\rm IR}$ was calculated by using the *IRAS* four-band fluxes and the equation given in Sanders & Mirabel 1996), which comprise a flux-limited subset of the Great Observatories All-Sky LIRGs Survey sample (GOALS; Armus et al. 2009). The full program details as well as observational data on individual galaxies will be given in a future paper upon the expected completion of the program in early 2013. Here we present a subsample of 70 galaxies, including 63 LIRGs and 7 ULIRGs ($L_{\rm IR} > 10^{12}\ L_\odot$), all of which are point sources with respect to the *Herschel* SPIRE/FTS beam. The determination of these galaxies as relative point sources was based both on their observed mid-infrared emission extent (for example, see Díaz-Santos et al. 2010, 2011) and on the consistency between the observed emission strength seen in the overlapping FTS bands between 316 and 324 μm (beam sizes are $\sim 20''$ and $\sim 37''$ for SPIRE Short Wavelength Spectrometer Array (SSW) and SPIRE Long Wavelength Spectrometer Array (SLW), respectively, in this wavelength range). A companion letter (N. Lu et al. 2013, in preparation) gives a brief program description and some initial results on the observed CO line emission.

The observations were conducted with the SPIRE FTS in staring and high spectral resolution mode between 194 and 672 μm, yielding a resolution of 0.04 cm^{-1} (=1.2 GHz). The data were reduced using a customized version of the standard SPIRE reduction and calibration pipeline for point source mode included in HIPE version 7.3 (Ott 2010). We used an averaged telescope relative spectral response function (RSRF) in place of the daily RSRF, to perform the flux calibration. During the reduction, we did not apply any apodization to the spectra. To extract the final spectrum, a "background" emission, which was obtained by fitting the median spectrum from the spatially surrounding detectors, was subtracted from the central detector.

In most cases the [N II] 205 μm line is the brightest line in the SPIRE FTS wavelength range, and almost all sources show high signal-to-noise ratio (S/N) in the [N II] line. In Figure 1 we plot several typical spectra of the [N II] line for galaxies with a range of FIR colors ($0.4 \lesssim f_{60}/f_{100} \lesssim 1.4$), and superimpose a fitted continuum and the line profile. From the figure, one can see that the fixed *Sinc* function convolved with a free width Gaussian (SCG) profile gives a better fitting result for the [N II] line since the instrumental resolution of the SPIRE FTS in high resolution mode at $\sim$210 μm is only about 300 km s^{-1} and the line width has an influence on the line shape. Therefore, we adopted the SCG profiles for the integrated [N II] line flux measurements except for one galaxy (CGCG448-020) where a single *Sinc* profile was better due to its narrow line width (<200 km s^{-1} for low J CO lines, e.g., Baan et al. 2008; Leech et al. 2010) and relatively low S/N ($\sim$4) in the line. The resulting full width at half-maximum of the [N II] line (excluding CGCG448-020) is 140–610 km s^{-1}, with a median value of $\sim$300 km s^{-1}. In most cases, the 1σ statistical uncertainties in the integrated line flux are less than 10%, and the median value is 7%.

3. RESULTS AND DISCUSSIONS

3.1. $L_{[\rm N\,II]}$–$L_{\rm IR}$ Correlation

Our sample galaxies are all (U)LIRGs and 23 out of 70 show active galactic nucleus (AGN)/LINER features (identified using optical, mid-infrared, or X-ray data). In order to increase the size and dynamic range of the sample used to study the $L_{[\rm N\,II]}$–$L_{\rm IR}$ relation, we also include 30 unresolved galaxies observed by *ISO* LWS and compiled by Brauher et al. (2008) in our analysis. For these objects, most of which are normal star-forming galaxies, the luminosity distances were derived with the same method as used for our (U)LIRG sample (e.g., Armus et al. 2009), i.e., by correcting the heliocentric velocity for the three-attractor flow model of Mould et al. (2000). Their [N II] 205 μm fluxes are derived from the observed [N II] 122 μm fluxes given in Brauher et al. (2008), using the theoretical [N II] 122 μm to [N II] 205 μm emission ratio (hereafter R_{21}) at $n_e = 80$ cm^{-3} (the median value for late-type galaxies; see, e.g., Ho et al. 1997) of $R_{21} = 2.6$. Here we compute the theoretical R_{21} by assuming electron impact excitation for the ground-state levels of N^+, and using the fitted results (Draine 2011) of Hudson & Bell (2005) with $T = 8000$ K to calculate the collision strengths (more details are provided in Y. Zhao et al. 2013, in preparation). Regarding the inclusion of Brauher et al. galaxies in our study, we note that (1) about 90% of the galaxies in Ho et al. (1997) have $n_e < 300$ cm^{-3}, yielding a theoretical $R_{21} = 0.94\text{–}5.3$ ($n_e = 10\text{–}300$ cm^{-3}), (2) empirically, we see an observed R_{21} of 1.5–4.3 for the nine galaxies (eight in our sample plus M82) that have both [N II] 122 μm and [N II] 205 μm data. Therefore, the uncertainty in $L_{[\rm N\,II]}$ caused by extrapolating [N II] 205 μm fluxes from [N II] 122 μm emissions is a factor of a few ($\sim$0.3 dex), and is significantly smaller than

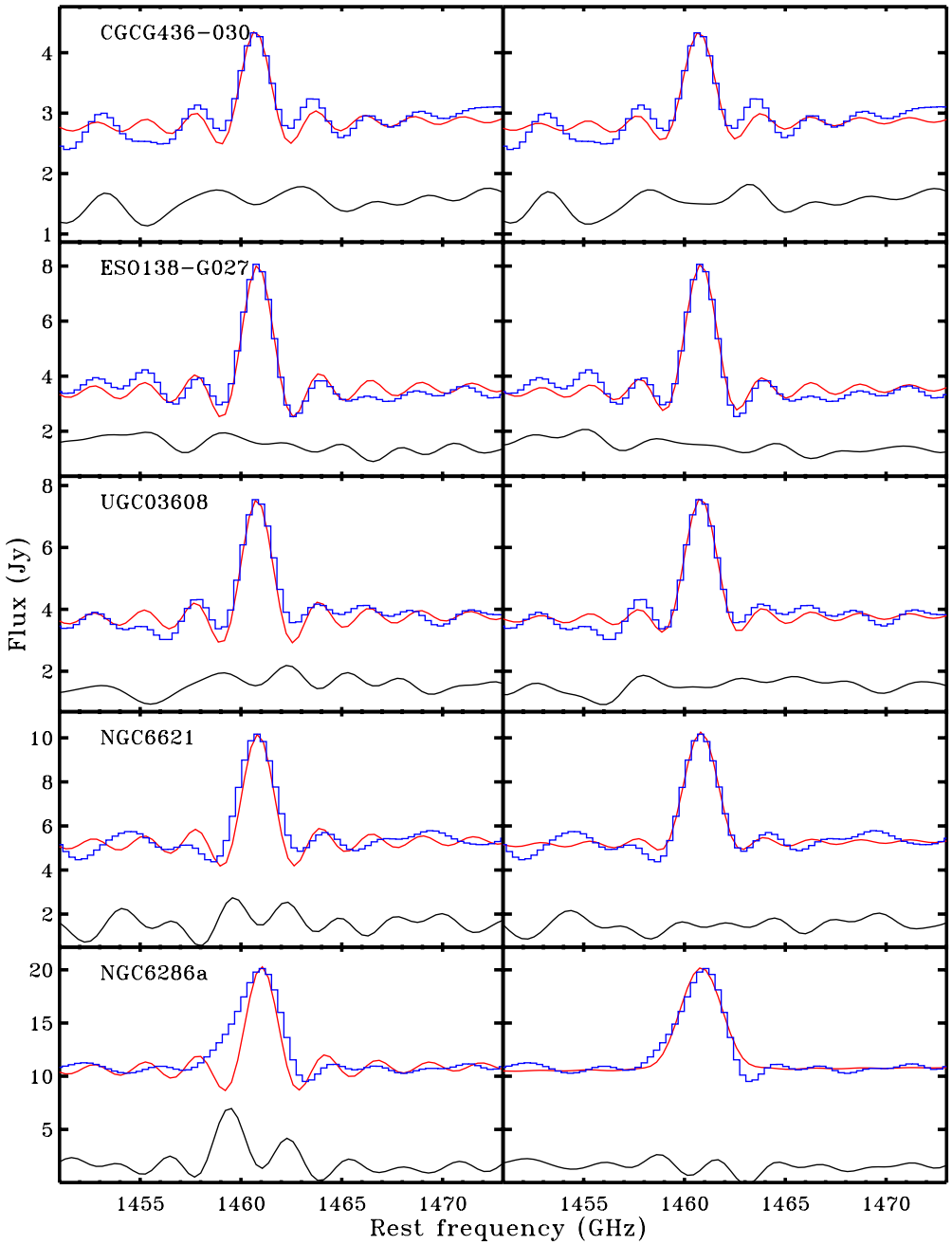

Figure 1. Typical spectra (corrected to the source rest frame) of the [N II] 205 μm line for galaxies with a range of f_{60}/f_{100} colors (going redder from top to bottom). In each panel, the blue, red, and black lines show the observed spectrum, the fitted profile of the [N II] line plus continuum, and the residual, respectively. In the left panels, the [N II] line is fitted using a *Sinc* function with a free width parameter. The right panels show the same data but the line is fitted using a fixed instrumental *Sinc* function convolved with a free width Gaussian (SCG) shape. It is clear that the SCG function can give a better fitting result for this line.

(A color version of this figure is available in the online journal.)

the two order-of-magnitude span of $L_{\rm IR}$ found in our sample, thus yielding useful results concerning the $L_{\rm [N\,II]}$–$L_{\rm IR}$ relation.

In Figure 2, we plot $L_{\rm [N\,II]}$ against $L_{\rm IR}$ for both our (U)LIRGs (circles) and Brauher et al.'s galaxies (diamonds), as well as the starburst galaxy M82 (star symbol; Petuchowski et al. 1994). The solid symbols indicate AGNs/LINERs. Generally, $L_{\rm [N\,II]}$ increases with $L_{\rm IR}$, albeit the scatter seems to increase with $L_{\rm IR}$ (we will return to this later). In fact, the scatter at the high $L_{\rm IR}$ end will be much reduced if we only look at the non-active galaxies. A non-weighted least-squares linear fit, using a geometrical mean functional relationship (Isobe et al. 1990), to the non-active galaxies, gives

$$\log L_{\rm IR} = (4.51 \pm 0.32) + (0.95 \pm 0.05) \log L_{\rm [N\,II]} \quad (1)$$

with a scatter of 0.26 dex in $L_{\rm IR}$. The Spearman rank correlation coefficient ρ of the trend is 0.78 at a $>5\sigma$ level of significance, which indicates a very strong correlation between $L_{\rm [N\,II]}$ and $L_{\rm IR}$. Our fit shows that, on average, $L_{\rm IR}$ scales with $L^{\alpha}_{\rm [N\,II]}$ with α between 0.8 and 1.1 at the 3σ significance. This nearly linear relation suggests that the power source of the [N II] 205 μm emission tightly relates to the star-forming activities. Using the SFR–$L_{\rm IR}$ calibration given in Kennicutt & Evans (2012), we can also build a direct relation between SFR and $L_{\rm [N\,II]}$, namely

$$\log {\rm SFR}\,(M_{\odot}\,{\rm yr}^{-1}) = (-5.31 \pm 0.32) + (0.95 \pm 0.05) \log L_{\rm [N\,II]}\,(L_{\odot}). \quad (2)$$

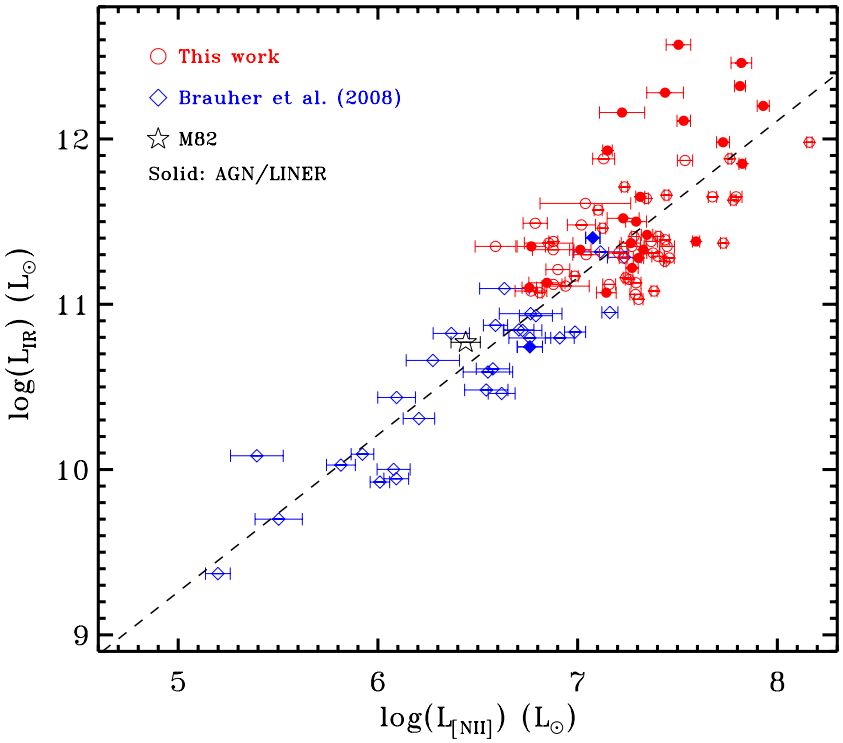

Figure 2. [N II] 205 μm plotted against total infrared luminosities for normal and luminous infrared galaxies. The circles (red) are galaxies having *Herschel* observations. The diamonds (blue) are galaxies from Brauher et al. (2008), for which an additional uncertainty of ∼0.3 dex should be taken into account besides the plotted error bar. The superposed line represents a geometrical mean, least-squares linear fit to all data points except for those solid symbols.

(A color version of this figure is available in the online journal.)

Comparing to the IR luminosity, the [N II] 205 μm emission could be a more convenient SFR indicator in the sense that it is more unambiguous, i.e., less affected by emissions from older stars (e.g., in the Milky Way the [N II] 205 μm flux is lower than that predicted by a linear $L_{[\rm N\,II]}$–$L_{\rm IR}$ relation when IR intensity going lower; see Figure 4 in Bennett et al. 1994), and inter-comparable since the techniques for obtaining $L_{\rm IR}$ for low- and high-redshift objects are so instrument-dependent. The majority of massive galaxies up to $z = 5$–6 are already chemically evolved systems based on their CO and dust emissions (Solomon & Vanden Bout 2005) or optical/IR line spectroscopy (Hamann & Ferland 1999). Therefore, Equation (2) can be reasonably applicable to high-z starburst galaxies despite that the $L_{[\rm N\,II]}$–$L_{\rm IR}$ relation possibly depends on metallicity.

3.2. The Scatter in the $L_{\rm IR}$–$L_{[\rm N\,II]}$ Relation

In Figure 2 we can also see an indication of a steeper relation between $L_{[\rm N\,II]}$ and $L_{\rm IR}$ for $L_{\rm IR} > 10^{11}\,L_\odot$ galaxies. This is more clearly demonstrated in Figure 3(a), in which we plot $L_{[\rm N\,II]}/L_{\rm IR}$ versus $L_{\rm IR}$ for the same set of galaxies. For ULIRGs, the mean $L_{[\rm N\,II]}/L_{\rm IR}$ (−4.69 dex) is considerably lower than that (−4.14 dex) of the galaxies with lower IR luminosities. Due to the small ULIRG sample size and the prevalence of AGN, we can reach no firm conclusion as to whether the $L_{[\rm N\,II]}/L_{\rm IR}$ decreases with $L_{\rm IR} > 10^{12}\,L_\odot$ for starburst-dominated galaxies.

However, the scatter in the $L_{\rm IR}$–$L_{[\rm N\,II]}$ relation is as large as ∼0.3 dex, and seems to increase with $L_{\rm IR}$, especially when ULIRGs are taken into account. The scatter could have several different origins: metallicity variations and, most likely, differing ionizing conditions. These latter effects include the stellar UV input via the initial mass function, the aging of starbursts, the H II region/ISM geometry, or the presence of an AGN. Our sample of galaxies contains few low-metallicity objects, and therefore we only address ionization effects here.

We note that the ionization parameter (U) can be especially high in (U)LIRGs (e.g., Farrah et al. 2007; Petric et al. 2011), where U is defined as the dimensionless ratio of the number density of incident ionizing photons to the number density of hydrogen nuclei. Clearly, U can be measured through ionization-parameter-sensitive line ratios, such as [O III]/[O II] and [N III]/[N II]. Moreover, theoretical models have also shown that U can be roughly indicated by the IR color, f_{60}/f_{100}, by the means that $\log U$ increases with f_{60}/f_{100} (see, e.g., Abel et al. 2009).

In Figure 3(b) we plot the dependence of $L_{[\rm N\,II]}/L_{\rm IR}$ on f_{60}/f_{100}. We can see from the figure that there only exists a very weak dependence of $L_{[\rm N\,II]}/L_{\rm IR}$ on f_{60}/f_{100} when $\log(f_{60}/f_{100}) < -0.2$. However, $L_{[\rm N\,II]}/L_{\rm IR}$ clearly decreases as f_{60}/f_{100} increases when $\log(f_{60}/f_{100}) \gtrsim -0.2$, except for a few galaxies with the warmest FIR colors in the sample. Moreover, the scatter in this correlation is less than that in the $L_{[\rm N\,II]}/L_{\rm IR}$ versus $L_{\rm IR}$ plot (see Figure 3(a)) and depends little on f_{60}/f_{100}. But we note that the scatter in the $L_{[\rm N\,II]}/L_{\rm IR}$–$f_{60}/f_{100}$ plot is still large, and we hypothesize that it is caused by the variations in the radiation field, since N^+ needs high energy (29.6 eV) to form N^{++}, and the population of ionic N is determined mainly by the slope of the background UV spectrum, i.e., the hardness, at a given U.

To try to account for the effects of the hardness of ionizing radiation field on $L_{[\rm N\,II]}/L_{\rm IR}$, we use the ratio of the [O III] 88 μm emission, rather than [N III] 57 μm emission where there are few detections, to the [N II] 205 μm emission to trace the hardness of the ionizing photons. It takes 35 eV to form O^{++}, which is

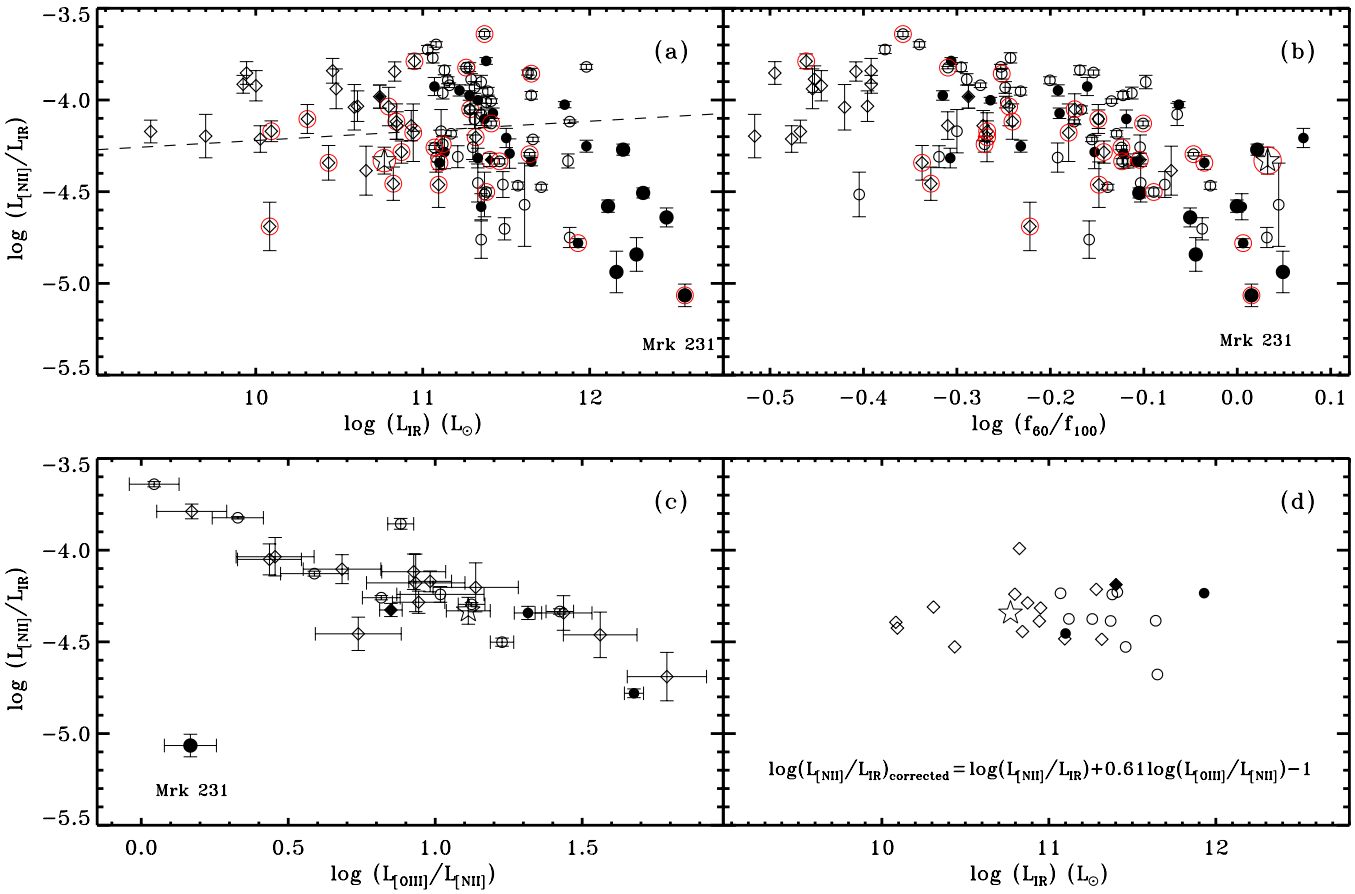

Figure 3. Ratio of [N II] 205 μm to IR luminosity is plotted against ((a) and (d)) IR luminosity, (b) *IRAS* 60 μm/100 μm color, and (c) [O III] 88 μm/[N II] 205 μm flux ratio. The symbols are the same as in Figure 2 except that here larger circles represent ULIRGs. The symbols enclosed by an additional red circle in panels (a) and (b) are the same sources as shown in panels (c) and (d). Equation (1) is shown by the dashed line in panel (a). The ordinate of panel (d) is a nominal value after the correction for the hardness effect (using the equation shown in this panel). Mrk 231 is outside the plotted range of panel (d).

(A color version of this figure is available in the online journal.)

only ∼5 eV higher than that needed for the formation of N^{++}, and thus the [O III]/[N II] line ratios are even stronger indicator of the hardness. Furthermore, this ratio is insensitive to the gas density (Rubin 1984). Except for M82 (Duffy et al. 1987) and Mrk 231 (Fischer et al. 2010), all of the [O III] 88 μm fluxes are adopted from Brauher et al. (2008).

Figure 3(c) shows the relation between $L_{[\mathrm{O\,III}]}/L_{[\mathrm{N\,II}]}$ and $L_{[\mathrm{N\,II}]}/L_{\mathrm{IR}}$. Clearly, there exists a good correlation such as $L_{[\mathrm{N\,II}]}/L_{\mathrm{IR}}$ decreases as $L_{[\mathrm{O\,III}]}/L_{[\mathrm{N\,II}]}$ increases. There is only one outlier, the ULIRG Mrk 231, which shows both small $L_{[\mathrm{N\,II}]}/L_{\mathrm{IR}}$ and $L_{[\mathrm{O\,III}]}/L_{[\mathrm{N\,II}]}$. Excluding Mrk 231, and using an ordinary least-squares linear fit to the data, we obtain $\log(L_{[\mathrm{N\,II}]}/L_{\mathrm{IR}}) = (-3.63 \pm 0.06) + (-0.61 \pm 0.06)\log(L_{[\mathrm{O\,III}]}/L_{[\mathrm{N\,II}]})$. The Spearman rank correlation coefficient ρ of this correlation is −0.93 at a $>5\sigma$ level of significance.

Galaxies plotted in Figure 3(c) (hereafter the [O III] sample) are also marked with red circles in Figures 3(a) and (b), which indicate that the hardness variation of the heating radiation field among galaxies can largely account for the scatter shown in the L_{IR}–$L_{[\mathrm{N\,II}]}$ relation, at least for $L_{\mathrm{IR}} < 10^{12}\ L_{\odot}$ galaxies. Actually, this is also supported by the fact that the scatter of less luminous galaxies (0.2 dex for Brauher et al. sample; thus probably less active in star formation and lower U) is smaller than that of our luminous sample (0.28 dex). Keeping in mind that the conversion from [N II] 122 μm flux to [N II] 205 μm flux may contribute largely to the scatter of Brauher et al. sample, the real scatter in the $L_{[\mathrm{N\,II}]}$–L_{IR} relation might probably be even smaller for these galaxies.

To obtain a direct view of how much the scatter can be reduced, we also display the hardness-corrected $L_{[\mathrm{N\,II}]}/L_{\mathrm{IR}}$, which was calculated according to the fitted $L_{[\mathrm{O\,III}]}/L_{[\mathrm{N\,II}]}$–$L_{[\mathrm{N\,II}]}/L_{\mathrm{IR}}$ relation, for the [O III] sample in Figure 3(d) (arbitrarily scaled). Comparing to Figure 3(a), one can see that the scatter is reduced significantly (from 0.26 dex to 0.11 dex by excluding Mrk 231, which is still an outlier due to that the hardness correction has little effect on it, and is outside the plotted range).

All of the seven ULIRGs in our sample show some deficit in $L_{[\mathrm{N\,II}]}$ relative to L_{IR}. Four of the seven, including Arp 220 and Mrk 231, were observed by *ISO* LWS, but no [O III] 88 μm emission was detected at the 3σ limit (e.g., Brauher et a. 2008), despite all showing some AGN characteristics. These galaxies also show very warm FIR colors (see Figure 3(b)). Therefore, very dusty H II regions with high U might be needed to explain the deficit of [N II] emission in these galaxies (e.g., Fischer et al. 1999; Abel et al. 2009; Draine 2011).

4. SUMMARY

In this Letter we have presented our initial results of the [N II] 205 μm emission for a sample of 70 (U)LIRGs observed by the *Herschel* SPIRE FTS. Combining with the *ISO* and *IRAS* data, we have studied the correlation between $L_{[\mathrm{N\,II}]}$ and L_{IR},

and investigated the dependence of $L_{[\mathrm{N\,II}]}/L_{\mathrm{IR}}$ on L_{IR}, FIR color f_{60}/f_{100}, and the UV hardness indicator [O III]/[N II]. The main conclusions of our work are as follows.

1. For star-forming galaxies with $L_{\mathrm{IR}} < 10^{12}\,L_{\odot}$, there exists a strong correlation between $L_{[\mathrm{N\,II}]}$ and L_{IR}, namely $\log L_{\mathrm{IR}} = (4.51 \pm 0.32) + (0.95 \pm 0.05) \log L_{[\mathrm{N\,II}]}$, implying that the [N II] emission can be used as an effective measure on SFR, particularly for sources where L_{IR} is difficult to measure such as high-z galaxies.
2. For galaxies with $L_{\mathrm{IR}} < 10^{12}\,L_{\odot}$ in our sample, the $L_{[\mathrm{N\,II}]}/L_{\mathrm{IR}}$ ratio is in the range of ~ -4.8 dex and ~ -3.6 dex, and varies systematically with the hardness/ionization parameter of the radiation field. However, additional effects are needed to explain the scatter in the $L_{[\mathrm{N\,II}]}$–L_{IR} relation and their relatively lower $L_{[\mathrm{N\,II}]}/L_{\mathrm{IR}}$ ratio for more IR luminous galaxies in our sample.

We thank the anonymous referee for comments which improved this manuscript. This work is based in part on observations made with *Herschel*, an European Space Agency Cornerstone Mission with significant participation by NASA. Support for this work was provided in part by NASA through an award issued by JPL/Caltech. Research for this project is partially supported by the Natural Science Foundation of China (grant 10833006) and Jiangsu Province (SBK201120678). Y.Z. thanks IPAC for the hospitality and the financial support during his visit. This research has made use of the NASA/IPAC Extragalactic Database (NED), which is operated by the Jet Propulsion Laboratory, California Institute of Technology, under contract with the National Aeronautics and Space Administration.

REFERENCES

Abel, N. P., Dudley, C., Fischer, J., Satyapal, S., & van Hoof, P. A. M. 2009, ApJ, 701, 1147
Armus, L., Mazzarella, J. M., Evans, A. S., et al. 2009, PASP, 121, 559
Baan, W. A., Henkel, C., Loenen, A. F., Baudry, A., & Wiklind, T. 2008, A&A, 477, 747
Bennett, C. L., Fixsen, D. J., Hinshaw, G., et al. 1994, ApJ, 434, 587
Brauher, J. R., Dale, D. A., & Helou, G. 2008, ApJS, 178, 280
Calzetti, D., Sheth, K., Churchwell, E., & Jackson, J. 2009, in 4th Spitzer Science Center Conf., The Evolving ISM in the Milky Way and Nearby Galaxies, ed. K. Sheth, A. Noriega-Crespo, J. Ingalls, & R. Paladini, available online at http://ssc.spitzer.caltech.edu/mtgs/ismevol/
Combes, F., Rex, M., Rawle, T. D., et al. 2012, A&A, 538, L4
Cui, X. 2010, HiA, 15, 639
Decarli, R., Walter, F., Neri, R., et al. 2012, ApJ, 752, 2
Díaz-Santos, T., Charmandaris, V., Armus, L., et al. 2010, ApJ, 723, 993
Díaz-Santos, T., Charmandaris, V., Armus, L., et al. 2011, ApJ, 741, 32
Draine, B. T. 2011, Physics of the Interstellar and Intergalactic Medium (Princeton, NJ: Princeton University Press)
Duffy, P. B., Erickson, E. F., Haas, M. R., & Houck, J. R. 1987, ApJ, 315, 68
Farrah, D., Bernard-Salas, J., Spoon, H., et al. 2007, ApJ, 667, 149
Fischer, J., Luhman, M. L., Satyapal, S., et al. 1999, Ap&SS, 266, 91
Fischer, J., Sturm, E., González-Alfonso, E., et al. 2010, A&A, 518, L41
Griffin, M. J., Abergel, A., Abreu, A., et al. 2010, A&A, 518, L3
Hamann, F., & Ferland, G. 1999, ARA&A, 37, 487
Ho, L. C., Filippenko, A. V., & Sargent, W. L. W. 1997, ApJ, 487, 579
Hudson, C. E., & Bell, K. L. 2005, A&A, 430, 725
Isobe, T., Feigelson, E. D., Akritas, M. G., & Babu, G. J. 1990, ApJ, 364, 104
Kennicutt, R. C., & Evans, N. J. 2012, ARA&A, 50, 531
Leech, J., Isaak, K. G., Papadopoulos, P. P., Gao, Y., & Davis, G. R. 2010, MNRAS, 406, 1634
Lord, S. D., Hollenbach, D. J., Colgan, S. W. J., et al. 1995, in ASP Conf. Ser. 73, Airborne Astronomy Symposium on the Galactic Ecosystem: From Gas to Stars to Dust, ed. M. R. Haas, J. A. Davidson, & E. F. Erickson (San Francisco, CA: ASP), 151
Mould, J. R., Huchra, J. P., Freedman, W. L., et al. 2000, ApJ, 529, 786
Nagao, T., Maiolino, R., De Breuck, C., et al. 2012, A&A, 542, L34
Oberst, T. E., Parshley, S. C., Stacey, G. J., et al. 2006, ApJL, 652, L125
Ott, S. 2010, in ASP Conf. Ser. 434, Astronomical Data Analysis Software and Systems XIX, ed. Y. Mizumoto, K.-I. Morita, & M. Ohishi (San Francisco, CA: ASP), 139
Paine, S., Blundell, R., Papa, D. C., Barrett, J. W., & Radford, S. J. E. 2000, PASP, 112, 108
Petric, A. O., Armus, L., Howell, J., et al. 2011, ApJ, 730, 28
Petuchowski, S. J., Bennett, C. L., Haas, M. R., et al. 1994, ApJL, 427, L17
Pilbratt, G. L., Riedinger, J. R., Passvogel, T., et al. 2010, A&A, 518, L1
Rubin, R. H. 1984, ApJS, 57, 349
Sanders, D. B., & Mirabel, I. F. 1996, ARA&A, 34, 749
Solomon, P. M., & Vanden Bout, P. A. 2005, ARA&A, 43, 677
Wright, E. L., Mather, J. C., Bennett, C. L., et al. 1991, ApJ, 381, 200
Yang, H., Kulesa, C. A., Walker, C. K., et al. 2010, PASP, 122, 490